JBC Papers in Press. Published on February 1, 2017 as Manuscript M116.771204
The latest version is at http://www.jbc.org/cgi/doi/10.1074/jbc.M116.771204

Structural Analysis Reveals the Deleterious Effects of Telomerase Mutations in Telomerase-Associated Bone Marrow Failure Syndromes

Hunter Hoffman[a], Cory Rice[a,b] and Emmanuel Skordalakes[a,b]

[a]*Dept of Gene Expression and Regulation, The Wistar Institute, 3601 Spruce St, Philadelphia PA 19104*

[b]*Dept of Biochemistry and Molecular Biophysics, 3700 Hamilton Walk, Perelman School of Medicine, University of Pennsylvania, Philadelphia PA 19104*

Running title: Telomerase mutations associated with Bone Marrow Failure Syndromes impair binding of nucleic acid substrates

To whom correspondence should be addressed: Emmanuel Skordalakes, Department of Gene Expression and Regulation, The Wistar Institute, 3601 Spruce St, Philadelphia PA 1910 (skorda@wistar.org).

Keywords: Telomerase, Nucleic acid binding, X-ray crystal structure, Bone marrow failure syndromes

ABSTRACT

Naturally occurring mutations in the ribonucleoprotein reverse transcriptase, telomerase, are associated with the bone marrow failure syndromes dyskeratosis congenita (DKC), aplastic anemia (AA), and idiopathic pulmonary fibrosis (IPF). However, the mechanism by which these mutations impact telomerase function remains unknown. Here we present the structure of the human telomerase c-terminal extension (CTE or thumb domain) determined by the method of single-wavelength anomalous diffraction (SAD) to 2.31 Å resolution. We also used direct telomerase activity and nucleic acid binding assays to explain how naturally occurring mutations within this portion of telomerase contribute to human disease. The single mutations localize within three highly conserved regions of the telomerase thumb domain referred to as motifs E-I, (thumb loop and helix) E-II and E-III (the FVYL pocket, comprising the hydrophobic residues F1012, V1025, Y1089 and L1092). Biochemical data shows that the mutations associated with DKC, AA and IFP disrupt the binding between telomerase's protein subunit reverse transcriptase (TERT) and its nucleic acid substrates leading to loss of telomerase activity and processivity. Collectively our data shows that although these mutations do not alter the overall stability or expression of TERT, these rare genetic disorders are associated with an impaired telomerase holoenzyme that is unable to correctly assemble with its nucleic acid substrates, leading to incomplete telomere extension and telomere attrition, which are hallmarks of these diseases.

INTRODUCTION

Human telomerase is a ribonucleoprotein reverse transcriptase that replicates the ends of eukaryotic chromosomes (1). The protein subunit, TERT, consists of several domains (TEN, TRBD, RT (Fingers, Palm) and thumb) organized into a closed, ring configuration, generating a large cavity in the interior of the ring and where the RNA template and the DNA bind during telomere elongation (2-5). The closed configuration of the TERT ring is stabilized by extensive interactions between the thumb and TRBD domains as well as by protein - RNA interactions (3,6).

Several invariable motifs in the interior cavity of the TERT ring coordinate the RNA template and telomeric overhang (RNADNA hybrid) and position the 3'end of the DNA for catalysis (2,3). These include motifs E-I and E-II of the thumb domain, which bind the RNADNA hybrid and stabilize the telomerase elongation complex (2,7); the primer grip region which guides the DNA at the active site of the enzyme and motifs 2 and B' of the fingers and palm domain respectively, which position the RNA template above the active site of the enzyme for nucleotide binding and selectivity (2,3).

Current evidence shows that the RNA binding domain of telomerase (TRBD) binds the

template boundary element (TBE) and the activation domain (CR4/5) of TER (8-12). The TBE is a stem loop located only a few nucleotides upstream of the RNA template and is coordinated by the T, CP and CP2 motifs in *Tetrahymena thermophilla* (13,14) or T, CP and TFLY in vertebrates (8). These TBE-binding motifs are located at the interface of the TRBD and fingers domains and together they form a well-defined indentation on the surface of the protein providing the platform for a network of non-specific interactions with the TBE (13). Binding of the TBE to TRBD positions the RNA template at the active site of the enzyme thus promoting nucleotide binding and selectivity (3). We previously proposed, and it was subsequently shown that the TRBD-TBE interaction provides the steric block that prevents TERT from replicating beyond the 5'-end of the RNA template thus promoting telomerase repeat addition processivity (RAP) (2,4,13).

The telomerase activation domain consists of the stem loops P6a/b, P6.1 and P5 (15) and is coordinated by the VSR motif of TRBD and motifs E-II and E-III (FVYL pocket) of the thumb domain (6,9,10). Although CR4/5 is primarily coordinated by the TRBD, its stem loop P6.1 extends across the TRBD-Thumb interface and binds the FVYL pocket of the thumb domain (6). Extensive interactions between the CR4/5 and the terminal domains of the TERT ring most likely stabilize the telomerase ribonucleoprotein (RNP) complex and lock the closed ring configuration of TERT during telomere elongation.

Several naturally occurring mutations within the thumb domain contribute to the rare genetic disorders dyskeratosis congenita (DKC), aplastic anemia (AA), and idiopathic pulmonary fibrosis (IPF). Except for AA, which is acquired, these disorders are inherited in an autosomal dominant pattern (16-19). DKC affects multiple parts of the body including nail shape and growth, skin discoloration and oral leukoplakia (20-22). Patients affected by DKC may also develop aplastic anemia, a bone marrow failure disorder that interferes with the production of normal levels of red blood cells (23). DKC patients are also high risk for IPF, a disease associated with lung scaring and decrease in oxygen transport to the body (24). In addition to AA and IPF, DKC patients are also high risk cases for cancers of the neck, head, genitals and anus. In its most severe form, DKC patients develop Hoyeraal Hreidaarsson syndrome usually associated with an unusually small cerebellum and impairment of motor skills (25).

Here we report the structure of the human telomerase thumb domain and explain the role of the naturally occurring mutations in human disease. The structure reveals that most these mutations localize to the nucleic acid binding regions of the protein, which includes motifs E-I, E-II and E-III. Biochemical assays show that these disease-associated mutations interfere with proper telomerase elongation complex formation leading to telomere attrition and loss of cell viability.

RESULTS

Structure of the human telomerase thumb domain. We identified a construct of the human telomerase thumb domain (hThumb) consisting of residues 961-1132 by limited proteolysis (Fig. 1A). A longer construct consisting of residues 941-1132, which contains the thumb loop, a portion of motif E-I (3), produced low protein yields sufficient for biochemical but not crystallographic studies. We subsequently solved the structure of hThumb 961-1132 to 2.31 Å resolution using the method of single-wavelength anomalous dispersion (SAD) and a mercury derivative (Table 1). The structure revealed clear density for residues 965-1122 (Fig. 1C). The structure is an all helical bundle (Fig. 1B and D) and is structurally conserved with the *tribolium* telomerase thumb domain (tcThumb - RMSD 2.5 Å) (Fig. 1E and F). Within this domain there are three conserved motifs (E-I, E-II and E-III, Fig. 1B and C) involved in nucleic acid binding (2,3). Of note is the displacement of part of motif E-I by the same helix of a crystallographic symmetry related molecule (Supplemental Fig. 1A and B). The flexibility of a small portion of E-I of the isolated thumb domain can be attributed to the absence of contacts with the TRBD domain observed in the full length TERT, which stabilize this motif (2,3). Occupation of the displaced helix by a crystal symmetry related one, further confirms the structural and functional conservation of this helix in telomerases across species.

Another highly conserved region of the hThumb is the FVYL pocket formed by the loops that connect motifs E-I, E-II and E-III and was previously suggested to bind the P6.1 stem loop of

CR4/5 (6). The FVYL pocket is located at the interface of the TRBD - thumb domain and is approximately 12 Å away from the nearest TRBD residue. The human FVYL pocket is the result of a small gap, generated by the organization of the tips and connecting loops of helices α2, α3, and α4, α5 (Fig. 1B and D). The organization of the tips of these helices generates a gap 14 Å wide and 8 Å deep and is sufficient to accommodate 2-3 nucleotide bases. The solvent exposed, hTERT loop that connects helices α2 and α3 makes extensive interactions with the TRBD and contributes to the closed ring TERT configuration. In the absence of contacts with TRBD this loop is flexible with V1025 partially occupying the FVYL pocket (Fig. 1B and D). It is worth noting that the high salt crystal growth conditions may have also facilitated binding of V1025 into this hydrophobic region of the protein.

hThumb disease mutations disrupt protein-nucleic acid binding. To better understand the role of hThumb mutations in human disease we tested the ability of these mutant proteins to bind an RNADNA hybrid (hRNADNA) consisting of the human telomerase RNA template (CUAACCCU) and telomeric DNA (AGGGTTAG). To perform these assays, we overexpressed and purified to homogeneity the hThumb WT and R972H, R979W, C1015R, L1019F V1025F, N1028H, K1050E and V1090M mutant proteins. We tested these proteins for binding to the hRNADNA hybrid using fluorescence polarization (FP) assays. It is worth noting that the V1025F mutant protein appears to aggregate in solution when overexpressed as an independent domain and therefore we were unable to obtain a reliable Kd for this protein. The WT, hThumb binds the hRNADNA hybrid with approximately 450 nM binding affinity (Fig. 2A, B and Supplemental Table 2). The mutant proteins located in motif E-I and E-II and make direct contacts with the hRNADNA hybrid (R972H, R979W and K1050E) showed significantly lower affinity (2.6, 4 and 2.4 fold) for the hRNADNA hybrid than the WT protein. Similarly, the C1015R mutant which contributes to the structural organization of this region of the protein, and therefore the binding of the hRNADNA hybrid also showed significantly lower affinity for the hRNADNA hybrid (4.6 fold) than the WT protein. Surprisingly, the L1019F showed almost wild type affinity for the hRNADNA hybrid (1.3 fold) compared to the WT protein (Fig. 2A, B and Supplemental Table 2). Contrary to the mutations that contribute to hybrid binding, N1028H and V1090M showed a slight (1.5 fold) decrease in hRNADNA binding affinity, which is within the margin error. It is worth noting that in the full length TERT, the hRNADNA hybrid makes additional contacts with the TRBD and RT domains (2,6). We therefore expect a higher affinity for the hRNADNA in the context of the full length protein consistent with what has been previously reported (26).

hThumb disease mutations impair telomerase activity and processivity. We then asked how the disease associated mutations affect the activity and processivity of telomerase. To address this question, we performed direct telomerase activity assays. As a source of telomerase, we used lysates of HEK293T cells transfected with the plasmids pcDNA6-hTERT and pBS-U1-hTER overexpressing telomerase (*Plasmids were a gift form Joachim Lingner's laboratory, The Swiss Institute for Experimental Cancer Research*). Prior to carrying out the telomerase activity assays we checked the levels of WT and mutant hTERT in cell lysates. We did so by western blot analysis, using a hTERT, specific antibody (abx120550, Abbexa (27)), as described previously in Bryan et al. (6). Western blot analysis showed that all hThumb WT and mutant proteins (R972H, K1050E, V1025F, N1028W) express at nearly WT levels with subtle differences between them (Fig. 3A). The final activity and processivity of WT and mutant telomerases were adjusted for the subtle differences observed in the protein levels expressed and were quantified as previously described by Latrick, C.M. et al (28) (Details of activity and processivity quantification can be found in the methods section of the manuscript – Supplemental Fig. 2).

Depending on the severity of the TERT mutations, some mutant proteins show modest loss of telomerase activity and processivity, while others render the enzyme almost inactive (Fig. 3B). Mutations that make direct contacts with the hRNADNA hybrid or are important for the organization of these motifs show the most sever defects in telomerase activity and processivity. These include R972H and R979W of motif E-I and K1050E of motif-II (Fig. 4A-C). R972H and

K1050E show 2-fold loss of activity and processivity each, relative to the WT telomerase. The severe R979W mutation results in 4-fold loss of activity and 20% of processivity compared to the WT enzyme (Fig. 3B-D).

The TERT mutants C1015R and L1019F, which comprise part of motif E-I are in proximity to each other and are buried in the core of the protein. These two TERT mutations have significantly different effects in telomerase activity and processivity. C1015R shows 4-fold loss of activity and 20% loss of processivity relative to the wild type enzyme. In contrast, L1019F is almost 50% active compared to the WT enzyme while its processivity is WT-like (Fig. 3B-D).

The TERT mutations V1025F and N1028H comprise part of the loop that connects motifs E-I and E-II, while V1090M is part of motif EIII and they all form part of the FVYL pocket. These mutant proteins show a variety of changes in activity and processivity when compared to the WT protein. V1025F is 20% active and 70% processive relative to the WT telomerase; N1028H is 40% active while its processivity is almost WT (90%); and V1090M is 80% active and processive when compared to the WT enzyme (Fig. 3B-D). Interestingly, A1062T shows WT activity and processivity within the margin of error.

DISCUSSION

To better understand the role of the naturally occurring telomerase mutations associated with the bone marrow failure syndromes DKC, AA, and IPF we solved the structure of human telomerase thumb domain and performed a host of biochemical assays all geared toward understanding how these mutations affect telomerase function. The hThumb structure is structurally conserved to the *tribolium* thumb domain (tcThumb) (Fig. 1D and E), supporting structural conservation across species. The structural similarity between the two proteins allowed us to generated a telomerase model consisting of an overlay between the tcTERT - hRNADNA complex (PDB ID: 3KYL) and the hThumb domain (Fig. 4A). The overlay places the hThumb motifs E-I and part of motif E-II in the interior cavity of the TERT ring, where the hRNADNA hybrid binds (Fig. 4A). There are three residues within these two motifs implicated in DKC. These include R972H, R979W and K1050E. The charged side chains of R972 and R979 of motif E-I and K1050 of motif E-II extend toward the center of the TERT ring where the hRNADNA hybrid is located (Fig. 4B). R979 is within coordinating distance of the hRNADNA hybrid. R972 and K1050 are around 5.5Å from the nearest nucleic acid residue, which is sufficient for solvent mediated coordination. Alternatively, a slight structural rearrangement of the nucleic acid or of motif E-I and E-II could place the R972 and K1050 side chains within direct coordinating distance of the hRNADNA hybrid. Altering the long positively charged side chain of R972 and R979 into the shorter, bulkier histidine or tryptophan side chains would most likely disrupt the canonical contacts with the nucleic acid substrate thus interfering with telomerase function. In fact, the proximity of R979 to the RNA-DNA hybrid suggests that the large tryptophan side chain may interfere with productive telomeric DNA binding and telomerase, elongation complex assembly. Consistent with this hypothesis R972H and R979W show 2.6 and 4-fold loss of hRNADNA binding affinity respectively relative to the WT enzyme (Fig. 3B-D). Partial disruption of TERT - nucleic acid for R972H and K1050E leads to 50% loss of WT telomerase activity and processivity (Fig. 4A-C). The more severe R979W TERT mutant shows 80% and 20% loss of WT activity and processivity respectively (Fig. 3 and 4).

Interestingly, the mutant TERT A1062T does not affect telomerase function. A1062T shows nearly wild type telomerase activity and processivity (Fig. 3B-D). The biochemical data is further supported by the structure, which shows that A1062T is located at a solvent exposed loop region of hThumb (Fig. 4C) and is at least 15 Å away from the nearest known functional site of TERT. Consistent with this hypothesis, it has been proposed that this mutation is also present in healthy subjects with telomere length within the normal range (16). It has therefore been proposed that this mutation may be a rare polymorphism, which does not contribute to the development of bone marrow failure.

Two additional mutations associated with AA and IPF are C1015R and L1019F respectively. C1015 and L1019 comprise part of helix α2 of motif E-I, (Fig. 1B, C and 5A). These residues are involved in direct interactions with helix α1, which contains R972 and R979, the two hThumb residues involved in interactions with the hRNADNA.

Unlike R972 and R979, C1015 and L1019 are buried within the core of hThumb and are not in contact with the nucleic acid substrate (Fig. 5B). Specifically, C1015 is coordinated by the hydrophobic side chains of M970 and L974 (Fig. 5B), while L1019 is located adjacent to C1015 and coordinated by M970 and F1032 (Fig. 5B). Both residues are critical for the organization and positioning of helix α1 and possibly of the FVYL pocket. Substitution of these two residues with larger side chains would influence the overall organization of the tertiary structure of hThumb and of helix α1, which in turn would affect the fold of the protein and TERT nucleic acid binding. Consistent with this hypothesis C1015R shows sever loss (4.6 fold lower than the WT protein) of nucleic acid binding (Fig. 2A-C), and telomerase activity and processivity (4-fold loss of activity and 20% loss of processivity compared to the WT enzyme) (Fig. 3B-D). Our data is further supported by telomere length studies on peripheral blood mononuclear cells (PBMCs) from patients carrying the C1015R TERT mutation. Southern blot analysis of PBMCs from these patients showed marked telomere shortening frequently associated with low levels of telomerase or a dysfunctional telomerase holoenzyme (18). In contrast to C1015R, substitution of the branched leucine (L1019) side chain with the aromatic side chain of phenylalanine may be less disruptive to the fold of the protein. This is reflected in the WT binding affinity of this mutant TERT protein for the hRNADNA and its WT processivity compared to the WT enzyme (Fig. 3B-D). Close inspection of the L1019F binding site shows that it can accommodate the larger phenylalanine side chain with some subtle (if any) rearrangement of the side chains of the surrounding residues (Fig. 5B). However, the L1019F mutant shows 50% loss of WT telomerase activity, a defect that most likely contributes to IPF associated with this mutant.

The telomerase FVYL pocket is also contained within this domain, comprises one of the two most conserved regions of hThumb (Consurf) (29) and most likely binds the P6.1 stem loop of the activation domain of telomerase (6). Three reported disease mutations (V1025F, N1028H, and V1090M) are located within this pocket of hThumb. We discussed some of these mutations previously in the context of the telomerase model published in PNAS (6,30). With the hThumb structure at hand we want to point out that these mutations indeed form part of the FVYL pocket of TERT (Fig. 5C). The precise mechanism of action of these mutations in telomerase function can only be obtained in the presence of a structure of hThumb bound to the P6.1 stem loop of CR4/5. However, we decided to test if these mutations influence hRNADNA binding. As we mentioned in the results section of the manuscript V1025F most likely aggregates in solution and we could not obtain an accurate Kd. However, FP assays of N1028H and V1090M show a subtle change in hRNADNA binding affinity (≤1.5 fold) compared to the WT enzyme (Fig. 2A, B and Supplemental Table 2). This is not surprising as these two residues (N1028H and V1090M) comprise part of the loops that connect helices α2-α3 and α4-α5 respectively (Fig. 5C). They are located >20 Å away from the hRNADNA binding site and are not involved in the structural organization of this domain. The subtle changes in hRNADNA binding combined with the effect on P6.1 binding potentially explains the detrimental effects of these mutations in telomerase function and the development of the bone marrow failure associated diseases.

Taken together our data suggest that the disease associated mutations discussed here do not alter the overall stability or expression of TERT, but instead, they are preventing proper nucleic acid interactions resulting in significant decrease in telomerase activity and processivity. Consistent with the structural and biochemical assays, southern blot analysis of DNA extracted from total peripheral blood white cells of patients carrying these disease mutations showed significantly shorter telomeres, a chromosomal defect usually associated with impaired telomerase activity (19,31-33).

The role of TERT missense mutations associated with DC/AA/PF is very hard to establish because they are so rare. However, our structural and biochemical data provides significant insights into the role of these mutations in telomerase function and how they may contribute to human disease. Some of the main telomere associated characteristics of these rare genetic disorders are significantly reduced telomerase activity and short telomeres. The severity of the disease is directly related to the degree of telomere shortening, which can be attributed in part to a dysfunctional telomerase.

EXPERIMENTAL PROCEDURES

Protein Expression and Purification - The human thumb domain residues 961-1132 were cloned into a modified vector expressing a hexahistidine tag (His-tag) followed by a tobacco etch virus (TEV)-cleavable small ubiquitin-like modifier (SUMO) fusion protein at its N-terminus. The protein was overexpressed in *E. coli* ScarabXpress-1 (T7Lac) cells (Scarab Genomics) at 16º C overnight using 1 mM IPTG (isopropyl-β-D-thiogalactopyranoside; Gold Biotechnology). Cells were harvested by centrifugation and resuspended in buffer containing 25mM Tris-HCl (pH 7.5), 0.5M KCl, 5% glycerol, 0.1mM benzamidine, 0.1M PMSF and 15mM imidazole prior to lysis via sonication. The hThumb protein was then purified over a Ni-nitrilotriacetic acid resin (Ni.NTA; MCLab) column. The His-SUMO-tag was cleaved by TEV endopeptidase overnight at 4º C. We further purified the protein over a porous HS resin (Applied Biosystems) column using a gradient of 25 mM Tris-HCl (pH 7.5), 0.5-1.5 M KCl, 5% glycerol, and 1 mM DTT. The protein was then concentrated and passed over a Superdex S200 size exclusion chromatography column (GE Healthcare) to remove any aggregation before moving on to crystallization.

Protein Crystallization and Data Collection - For crystallization studies, the purified protein was concentrated to 10mg/mL and dialyzed in a buffer containing 5 mM $NaHPO_4$ pH7.5, 100 mM KCl, and 1 mM TCEP. Crystals appeared within 3 days in sitting drop trays containing 0.8 M Li_2SO_4, and 50 mM Bis-Tris pH 8.5 at 10º C. Crystal diffraction was significantly improved with the additives 1 mM GSH/GSSG and 3% 1,6-hexanediol. Native and derivative data were collected in house on a Rigaku MicroMax-007 HF rotating anode X-ray generator (wavelength 1.54178 Å) with VariMax optics and using a Saturn 944 HG CCD detector. Data were processed with XDS (34) (Table 1). Phases were determined using the single anomalous dispersion (SAD) method using a mercury derivative prepared by soaking the crystals with 1 mM methyl mercury chloride for 30 minutes. Four mercury sites were identified by AutoSolve as implemented in Phenix (35) followed by phase calculation, density modification and model building (Table 1). Phenix produced a partial model which we completed in COOT (36) and refined using REFMAC5 (37). Models where prepared in COOT using structural overlays and the figures were prepared with PYMOL(38).

Fluorescence Polarization (FP) Assays - We tested hThumb (WT and mutant) - hRNADNA binding using fluorescent polarization (FP) assays with the Envision Xcite Multilabel Plate Reader (Perkin Elmer). 20 µl binding reactions were carried out in a buffer containing 20 mM Hepes, pH 7.5, 100 mM KCl, 2 mM $MgCl_2$, 1 mM EDTA, 2 mM DTT, 1 mg/mL BSA, 5% v/v glycerol. The hRNADNA probe consisting of the human telomerase RNA template and telomeric DNA linked together by a stable tertraloop (italics) (rCrUrArArCrCrCrUrGrC*dTdTdCdG*dGdCdAdGdGdGdTdTdAdG) was purchased with a 5′ 6-FAM label from Integrated DNA technologies. The final probe concentration used was 2.5 nM, while the hThumb protein concentration ranged from 0 to 15 µM. We incubated the reactions at room temperature for 30 minutes and pipetted in triplicate into a black 384 well optiplate (PerkinElmer). The reactions were excited at 480 nm and the emissions measured at 535 nm wavelength. The milipolarization (mP) values were calculated by the Envision operating software (PerkinElmer). The data was fit and the binding constants were determined with a one-site fit all, nonlinear regression model using PRISM 5.0 (GraphPad Software, San Diego California USA, www.graphpad.com).

Cell Culture - HEK293T cells were grown in DMEM (Gibco) and 10% fetal bovine serum (Gibco). WT and mutant pcDNA6-hTERT and WT pBS-U1-hTER were transfected in a 1:3 ratio into confluent cells following the standard Lipofectamine Transfection Reagent protocol (Thermo Fisher Scientific) as previously described by Cristofari , G. et. al. (39). The following day, cells were transferred to a t25 flask and allowed to grow for an additional day. Two days post transfection cells were trypsynized, pelleted and stored at -80º C until needed.

Western Blot Analysis - For the western blot analysis, standard immunoblot protocols (40) were used with the following antibody dilutions: anti-human TERT antibody (Abbexa, product number: 120550 (27), 1:1000 dilution), anti-β Actin antibody conjugated to HRP (Abcam, product number: 49900, 1:1000 dilution), and secondary HRP-conjugated anti-sheep IgG antibody (Santa

Cruz Biotech product number: 2924, 1:1000 dilution) used to detect the human TERT antibody. Detection of antibody signal was done with chemiluminescence activated using 2 mL of Luminata Forte Western HRP Substrate (Millipore). The signal was detected and developed with a Fuji LAS-3000 scanner. Western blot signals were quantified using ImageQuant TL (GE Healthcare) and normalized using the β-Actin signal as a loading control.

Direct Telomerase Assay - Total cell lysates were prepared using 1xCHAPS lysis buffer (150 mM KCl, 50 mM Tris-HCl pH 7.5, 1 mM MgCl2, 1 mM EGTA, 0.5% CHAPS, 10% glycerol, supplemented with protease inhibitor cocktail and 5 mM β-mercaptoethanol). Endogenous, WT, and mutant lysates containing 2μg of total protein were incubated in a Direct Assay reaction mix (50mM Tris-HCl pH 8, 50 mM KCl, 1mM $MgCl_2$, 1mM Spermidine, 5 mM β-mercaptoethanol, 0.04 mM dGTP, 0.5 mM dTTP, 0.5 mM dATP, 32U RNasin, 1 μM hTel Substrate TTAGGGTTAGCGTTAG GG) for 1 hr at 30º C. After incubation, had finished, 10 nmol of a ^{32}P-labelled loading control (single-stranded, yeast telomeric DNA, 10 bases long) was added to each sample. DNA was isolated by overnight precipitation in 3.6 M NH_4OAc pH 5, glycogen, and 100% ethanol at -80º C. The following day, DNA was pelleted and resuspended in 20 μL of gel loading buffer (98% formamide, 10 mM EDTA and 0.05% xylene cyanol) and incubated at 95º C for 5 minutes. Samples were then run on a 10% polyacrylamide (19:1), 8 M urea gel for 2 hours at 1800 V. The gel was then fixed with a 30% methanol, 10% acetic acid solution and vacuumed-dried at 80º C for 1 hour. The gel was exposed to phosphor storage plate overnight and imaged the following day.

Direct Assay Quantification - The direct telomerase assays were quantified as described previously (28,41). Briefly, the activity of each protein (WT or mutant) was determined as follows: We used Iamgequant TL (GE Healthcare) to determine the intensity of each band on the gel. The total intensity of each sample was adjusted based on the loading control. The intensity of each band was normalized for the number of radiolabeled nucleotides added per repeat. The total lane counts (TLCs) were then measured by taking the sum of the normalized band intensity over the entire lane.

The telomerase processivity for the WT and mutant hTERT proteins was quantified as follows: The intensity of each repeat was quantified using Imagequant and normalized by dividing by the total number of hot Gs incorporated per repeat number. For each repeat (x), the number of telomeric products not extended (or fraction left behind - FLB) was calculated by dividing the total intensity of bands (1-x) by the total counts from that lane. We then plotted the natural log of 1-FLB against each repeat number and the slope (m) from the linear regression (Supplemental Fig. 2) of this graph was used to determine the processivity of each telomerase (WT or mutant), by dividing -ln(2)/m.

Acknowledgements: We would like to thank *Dr. Joachim Lingner* for providing the Super-telomerase plasmids. The research was funded by the NIH grant R01CA201312 and the Wistar Cancer Center Support Grant P30 CA10815.

Conflict of interest: The authors declare that they have no conflicts of interest with the contents of this article.

Author contributions: ES and HH designed the experiments and wrote the manuscript. HH carried out the structural studies and telomerase activity assays. CR carried out the nucleic acid binding studies.

REFERENCES

1. Greider, C. W., and Blackburn, E. H. (1987) The telomere terminal transferase of Tetrahymena is a ribonucleoprotein enzyme with two kinds of primer specificity. *Cell* **51**, 887-898
2. Mitchell, M., Gillis, A., Futahashi, M., Fujiwara, H., and Skordalakes, E. (2010) Structural basis for telomerase catalytic subunit TERT binding to RNA template and telomeric DNA. *Nat Struct Mol Biol* **17**, 513-518
3. Gillis, A. J., Schuller, A. P., and Skordalakes, E. (2008) Structure of the Tribolium castaneum telomerase catalytic subunit TERT. *Nature* **455**, 633-637
4. Mason, M., Schuller, A., and Skordalakes, E. (2011) Telomerase structure function. *Curr Opin Struct Biol* **21**, 92-100
5. Sauerwald, A., Sandin, S., Cristofari, G., Scheres, S. H., Lingner, J., and Rhodes, D. (2013) Structure of active dimeric human telomerase. *Nat Struct Mol Biol* **20**, 454-460
6. Bryan, C., Rice, C., Hoffman, H., Harkisheimer, H., Sweeny, M., and Skordalakes, E. (2015) Structural Basis of Telomerase Inhibition by the Highly Specific BIBR1532 *Structure* **23**, 1-9
7. Huard, S., Moriarty, T. J., and Autexier, C. (2003) The C terminus of the human telomerase reverse transcriptase is a determinant of enzyme processivity. *Nucleic acids research* **31**, 4059-4070
8. Harkisheimer, M., Mason, M., Shuvaeva, E., and Skordalakes, E. (2013) A Motif in the Vertebrate Telomerase N-terminal Linker of TERT Contributes to RNA Binding and Telomerase Activity and Processivity. *Structure* **21**, 1-9
9. Huang, J., Brown, A. F., Wu, J., Xue, J., Bley, C. J., Rand, D. P., Wu, L., Zhang, R., Chen, J. J., and Lei, M. (2014) Structural basis for protein-RNA recognition in telomerase. *Nat Struct Mol Biol* **21**, 507-512
10. Bley, C. J., Qi, X., Rand, D. P., Borges, C. R., Nelson, R. W., and Chen, J. J. (2011) RNA-protein binding interface in the telomerase ribonucleoprotein. *Proceedings of the National Academy of Sciences of the United States of America* **108**, 20333-20338
11. Jiang, J., Miracco, E. J., Hong, K., Eckert, B., Chan, H., Cash, D. D., Min, B., Zhou, Z. H., Collins, K., and Feigon, J. (2013) The architecture of Tetrahymena telomerase holoenzyme. *Nature* **496**, 187-192
12. Jiang, J., Chan, H., Cash, D. D., Miracco, E. J., Ogorzalek Loo, R. R., Upton, H. E., Cascio, D., O'Brien Johnson, R., Collins, K., Loo, J. A., Zhou, Z. H., and Feigon, J. (2015) Structure of Tetrahymena telomerase reveals previously unknown subunits, functions, and interactions. *Science* **350**, aab4070
13. Jansson, L. I., Akiyama, B. M., Ooms, A., Lu, C., Rubin, S. M., and Stone, M. D. (2015) Structural basis of template-boundary definition in Tetrahymena telomerase. *Nat Struct Mol Biol* **22**, 883-888
14. Rouda, S., and Skordalakes, E. (2007) Structure of the RNA-binding domain of telomerase: implications for RNA recognition and binding. *Structure* **15**, 1403-1412
15. Chen, J. L., Blasco, M. A., and Greider, C. W. (2000) Secondary structure of vertebrate telomerase RNA. *Cell* **100**, 503-514
16. Alder, J. K., Chen, J. J., Lancaster, L., Danoff, S., Su, S. C., Cogan, J. D., Vulto, I., Xie, M., Qi, X., Tuder, R. M., Phillips, J. A., 3rd, Lansdorp, P. M., Loyd, J. E., and Armanios, M. Y. (2008) Short telomeres are a risk factor for idiopathic pulmonary fibrosis. *Proceedings of the National Academy of Sciences of the United States of America* **105**, 13051-13056
17. Calado, R. T., Regal, J. A., Hills, M., Yewdell, W. T., Dalmazzo, L. F., Zago, M. A., Lansdorp, P. M., Hogge, D., Chanock, S. J., Estey, E. H., Falcao, R. P., and Young, N. S. (2009) Constitutional hypomorphic telomerase mutations in patients with acute myeloid leukemia. *Proceedings of the National Academy of Sciences of the United States of America* **106**, 1187-1192
18. Du, H. Y., Pumbo, E., Ivanovich, J., An, P., Maziarz, R. T., Reiss, U. M., Chirnomas, D., Shimamura, A., Vlachos, A., Lipton, J. M., Goyal, R. K., Goldman, F., Wilson, D. B., Mason, P. J., and Bessler, M. (2009) TERC and TERT gene mutations in patients with bone marrow failure and the significance of telomere length measurements. *Blood* **113**, 309-316

19. Vulliamy, T. J., Kirwan, M. J., Beswick, R., Hossain, U., Baqai, C., Ratcliffe, A., Marsh, J., Walne, A., and Dokal, I. (2011) Differences in disease severity but similar telomere lengths in genetic subgroups of patients with telomerase and shelterin mutations. *PLoS One* **6**, e24383
20. Bessler, M., Wilson, D. B., and Mason, P. J. (2010) Dyskeratosis congenita. *FEBS letters* **584**, 3831-3838
21. Dokal, I. (1996) Dyskeratosis congenita: an inherited bone marrow failure syndrome. *Br J Haematol* **92**, 775-779
22. Kirwan, M., and Dokal, I. (2008) Dyskeratosis congenita: a genetic disorder of many faces. *Clin Genet* **73**, 103-112
23. Dokal, I., and Vulliamy, T. (2003) Dyskeratosis congenita: its link to telomerase and aplastic anaemia. *Blood Rev* **17**, 217-225
24. Tsakiri, K. D., Cronkhite, J. T., Kuan, P. J., Xing, C., Raghu, G., Weissler, J. C., Rosenblatt, R. L., Shay, J. W., and Garcia, C. K. (2007) Adult-onset pulmonary fibrosis caused by mutations in telomerase. *Proceedings of the National Academy of Sciences of the United States of America* **104**, 7552-7557
25. Knight, S. W., Heiss, N. S., Vulliamy, T. J., Aalfs, C. M., McMahon, C., Richmond, P., Jones, A., Hennekam, R. C., Poustka, A., Mason, P. J., and Dokal, I. (1999) Unexplained aplastic anaemia, immunodeficiency, and cerebellar hypoplasia (Hoyeraal-Hreidarsson syndrome) due to mutations in the dyskeratosis congenita gene, DKC1. *Br J Haematol* **107**, 335-339
26. Tomlinson, C. G., Holien, J. K., Mathias, J. A., Parker, M. W., and Bryan, T. M. (2016) The C-terminal extension of human telomerase reverse transcriptase is necessary for high affinity binding to telomeric DNA. *Biochimie*
27. Cohen, S. B., and Reddel, R. R. (2008) A sensitive direct human telomerase activity assay. *Nat Methods* **5**, 355-360
28. Latrick, C. M., and Cech, T. R. (2010) POT1-TPP1 enhances telomerase processivity by slowing primer dissociation and aiding translocation. *The EMBO journal* **29**, 924-933
29. Armon, A., Graur, D., and Ben-Tal, N. (2001) ConSurf: an algorithmic tool for the identification of functional regions in proteins by surface mapping of phylogenetic information. *J Mol Biol* **307**, 447-463
30. Steczkiewicz, K., Zimmermann, M. T., Kurcinski, M., Lewis, B. A., Dobbs, D., Kloczkowski, A., Jernigan, R. L., Kolinski, A., and Ginalski, K. (2011) Human telomerase model shows the role of the TEN domain in advancing the double helix for the next polymerization step. *Proceedings of the National Academy of Sciences of the United States of America* **108**, 9443-9448
31. Cronkhite, J. T., Xing, C., Raghu, G., Chin, K. M., Torres, F., Rosenblatt, R. L., and Garcia, C. K. (2008) Telomere shortening in familial and sporadic pulmonary fibrosis. *Am J Respir Crit Care Med* **178**, 729-737
32. Vulliamy, T. J., Walne, A., Baskaradas, A., Mason, P. J., Marrone, A., and Dokal, I. (2005) Mutations in the reverse transcriptase component of telomerase (TERT) in patients with bone marrow failure. *Blood Cells Mol Dis* **34**, 257-263
33. Yamaguchi, H., Calado, R. T., Ly, H., Kajigaya, S., Baerlocher, G. M., Chanock, S. J., Lansdorp, P. M., and Young, N. S. (2005) Mutations in TERT, the gene for telomerase reverse transcriptase, in aplastic anemia. *N Engl J Med* **352**, 1413-1424
34. Kabsch, W. (2010) Xds. *Acta Crystallogr D Biol Crystallogr* **66**, 125-132
35. Adams, P. D., Afonine, P. V., Bunkoczi, G., Chen, V. B., Davis, I. W., Echols, N., Headd, J. J., Hung, L. W., Kapral, G. J., Grosse-Kunstleve, R. W., McCoy, A. J., Moriarty, N. W., Oeffner, R., Read, R. J., Richardson, D. C., Richardson, J. S., Terwilliger, T. C., and Zwart, P. H. (2010) PHENIX: a comprehensive Python-based system for macromolecular structure solution. *Acta Crystallogr D Biol Crystallogr* **66**, 213-221
36. Emsley, P., and Cowtan, K. (2004) Coot: model-building tools for molecular graphics. *Acta Crystallogr D Biol Crystallogr* **60**, 2126-2132

37. Vagin, A. A., Steiner, R. A., Lebedev, A. A., Potterton, L., McNicholas, S., Long, F., and Murshudov, G. N. (2004) REFMAC5 dictionary: organization of prior chemical knowledge and guidelines for its use. *Acta Crystallogr D Biol Crystallogr* **60**, 2184-2195
38. Schrödinger, L. (Version 1.8) The PyMOL Molecular Graphics System.
39. Cristofari, G., Reichenbach, P., Regamey, P. O., Banfi, D., Chambon, M., Turcatti, G., and Lingner, J. (2007) Low- to high-throughput analysis of telomerase modulators with Telospot. *Nat Methods* **4**, 851-853
40. Palmer, H. M. (2000) Using Antibodies: A Laboratory Manual. *J. Antimicrob. Chemother.* **45**, 413-413
41. Wang, F., and Lei, M. (2011) Human telomere POT1-TPP1 complex and its role in telomerase activity regulation. *Methods in molecular biology* **735**, 173-187

FOOTNOTES

The coordinates and structure factors of the human telomerase thumb domain have been deposited in the Research Collaboratory for Structural Bioinformatics (RCSB) databank and the PDB ID number is 5UGW.

The abbreviations used are: Dyskeratosis congenita (DKC), aplastic anemia (AA), and idiopathic pulmonary fibrosis (IPF), ribonucleoprotein (RNP), Telomerase reverse transcriptase (TERT), Telomerase RNA (TER), C-terminal extension (CTE or thumb), Telomerase RNA binding domain (TRBD), Template boundary element (TBE), Telomerase RNA activation domain (CR4/5), TRBD RNA binding motifs (T, CP, CP2 and TFLY), repeat addition processivity (RAP).

FIGURES LEGENDS

FIGURE 1. Structure of the human TERT thumb (hThumb) domain. *A,* Primary structure of human TERT showing domains in distinct colors; Conserved motifs of the thumb domain are highlighted. *B*, X-ray crystal structure of the human Thumb (hThumb) domain. Motifs E-I, E-II E-III and E-IV are shown in green, blue, purple and red color respectively. *C*, Simulated-annealing omit map of residues 968-986 of motif E-I. *D,* Topology schematic of hThumb; same color scheme as that of panel *B*. *D,* Sequence alignment of human and *tribolium* thumb domains. *E,* Structural overlay of the human (salmon) and *tribolium* (limon) thumb domains.

FIGURE 2. WT and mutant hThumb RNA-DNA binding assays. *A,* Fluorescence polarization assays of hThumb WT and mutant (R972H, R979W, C1015R, L1019F, N1028H K1050E and V1090M) proteins with an RNADNA hybrid consisting of the human telomerase RNA template and telomeric DNA (hRNADNA – rCrUrArArCrCrCrUrGrC*dTdTdCdG*dGdC dAdGdGdGdT dTdAdG; the stable tertraloop is colored red). *B,* Bar graph showing the nucleic acid binding differences between the WT and mutant hThumb proteins. Ratio of mutant/WT hThumb, hRNADNA binding constants normalized to 1. All FP assays were carried out in triplicate and the average was used in these studies.

FIGURE 3. WT and mutant hTERT direct telomerase activity assays. *A,* Western blot analysis of hTERT WT and mutant (R972H, R979W, C1015R, L1019F, N1028H, K1050E, A1062T and V10190M) proteins overexpressed in HEK293T cells. *B,* Direct telomerase activity assay of WT and mutant hTERT telomerases. Lysates of HEK293T cells overexpressing telomerase (HEK293T cells transfected with pcDNA6-hTERT and WT pBS-U1-hTER) were used in the experiment. *C,* Quantification of WT and mutant hTERT telomerase activity (see methods section for details). *D,* Quantification of WT and mutant

hTERT telomerase processivity. The direct assays were carried out in duplicate and the numbers reported in this study are the average; the discrepancies between runs were used to calculate the error.

FIGURE 4. Model of hThumb - nucleic acid structure and location of R979H, R979W, K1050E and A1062T mutations. *A,* Overlay of the tcTERT-RNADNA hybrid (PDB:3KLY) and hThumb structures. Motifs E-I, E-II and E-III are highlighted in green, blue and purple color respectively. The mutations R979H, R979W, K1050E and A1062T are highlighted with a box. *B,* Model of hThumb in complex with the RNADNA hybrid rotated 90º along the X axis of the model in panel *A*. The model shows that R979H, R979W (green stick) and K1050E (purple stick) are involved in RNA template and telomeric DNA binding. *C,* Same model as in panel *B* rotated 90º along the Y axis of panel *A*. A1026T is shown in red stick. The position of A1062 in relationship to R979 (green stick) and K1050 (blue stick) are also shown. A1062 (red stick) is located at least 15 Å away from the nearest protein or nucleic acid binding region of the protein based on current evidence.

FIGURE 5. Model of hThumb - nucleic acid structure and location of C105R, L1019F, V1025F, N1028H and V1090M mutations. *A,* Overlay of the tcTERT-RNADNA hybrid (PDB:3KLY), the TRBD-CR4/5 (PDB:4O26) and hThumb structures. Motifs E-I, E-II and E-III are shown in green, blue and purple color respectively. The location of residues C1015R, L1019F, V1025F, N1028H and V1090M are highlighted with a box. *B,* Structure of hThumb rotated 45º along the Y axis of the model of panel *A*. The model shows that C1015 and L1019 (green stick) are buried in the core of hThumb and make direct contacts with hydrophobic residues (salmon stick) surrounding this region of the protein. ***C,*** Structure of hThumb rotated 90º along the Y axis of the model in panel *A*. The location of V1025F, N1028H and V1090M within the FVYL pocket containing motifs E-I, E-II and E-III and the coordinating residues are shown in color stick.

TABLES

Table 1: Data collection, phasing and refinement statistics

	Native	Phasing Hg Derivative 1
Data collection		
Wavelength (Å)	1.5418	1.5418
Space group	$P32_1$	$P32_1$
Cell dimensions		
a, *b*, *c* (Å)	92.4 50.2	92.9 49.9
Resolution (Å)	20-2.31 (2.25-2.31)	30-2.9 (3.05-2.9)
I/sI	18.7 (2.19)	12.3 (1.0)
Completeness (%)	99.9 (98.3)	99.6 (96.4)
Redundancy	12 (12.7)	28 (29.4)
Phasing Analysis		
Resolution (Å)		30-2.9
Number of sites		5
SKEW*: (Phenix)		0.20
CORR_RMS** (Phenix)		0.86
Mean figure of merit (FOM)		0.37
Refinement		
Resolution (Å)	20 - 2.31	
No. reflections	11191	
R_{work}/ R_{free}	20.0/21.6	
Estimated Twining fraction	0.358 for -h,-k,-l	
No. atoms		
Non-solvent	1289	
Water	12	
B-factors		
Protein	43.6	
Water	59.6	
R.m.s deviations		
Bond lengths (Å)	0.008	
Bond angles (°)	1.186	
Ramachandran plot (%)		
Most favored	97	
Allowed	3	

*SKEW – Distribution of electron density values in an experimentally phased map

**CORR_RMS - a measure of how contiguous the solvent and non-solvent regions are in the map

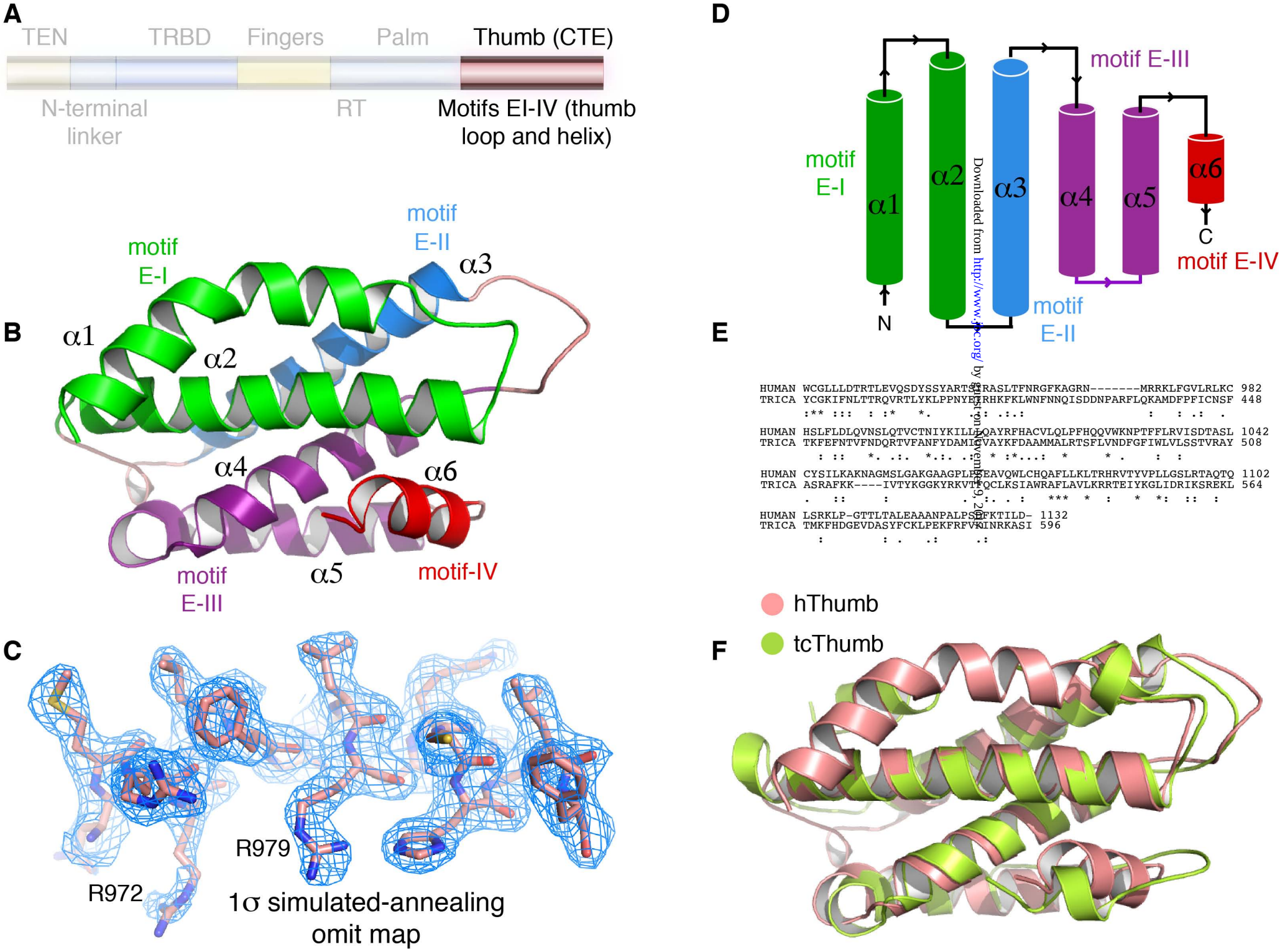
A
TEN
TRBD
Fingers
Palm
Thumb (CTE)
N-terminal linker
RT
Motifs EI-IV (thumb loop and helix)
B
motif E-I
motif E-II
α1
α2
α3
α4
α5
α6
motif E-III
motif-IV
C
R972
R979
1σ simulated-annealing omit map
D
motif E-I
motif E-III
motif E-II
motif E-IV
N
C
α1
α2
α3
α4
α5
α6
E
HUMAN WCGLLLDTRTLEVQSDYSSYARTSIRASLTFNRGFKAGRN-------MRRKLFGVLRLKC 982
TRICA YCGKIFNLTTRQVRTLYKLPPNYRRHKFKLWNFNNQISDDNPARFLQKAMDFPFICNSF 448
HUMAN HSLFLDLQVNSLQTVCTNIYKILLLQAYRFHACVLQLPFHQQVWKNPTFFLRVISDTASL 1042
TRICA TKFEFNTVFNDQRTVFANFYDAMIGVAYKFDAAMMALRTSFLVNDFGFIWLVLSSTVRAY 508
HUMAN CYSILKAKNAGMSLGAKGAAGPLPSEAVQWLCHQAFLLKLTRHRVTYVPLLGSLRTAQTQ 1102
TRICA ASRAFKK----IVTYKGGKYRKVTPQCLKSIAWRAFLAVLKRRTEIYKGLIDRIKSREKL 564
HUMAN LSRKLP-GTTLTALEAAANPALPSDFKTILD- 1132
TRICA TMKFHDGEVDASYFCKLPEKFRFVKINRKASI 596
Downloaded from http://www.jvi.org/ by guest on November 19, 2019
hThumb
tcThumb
F

Figure 1

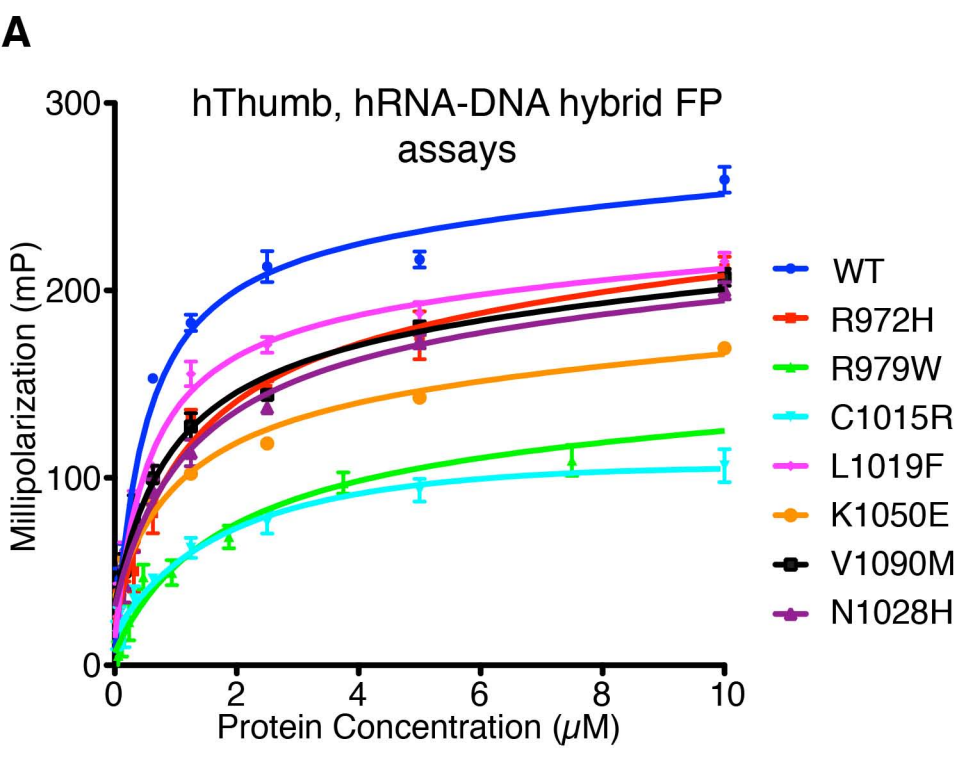

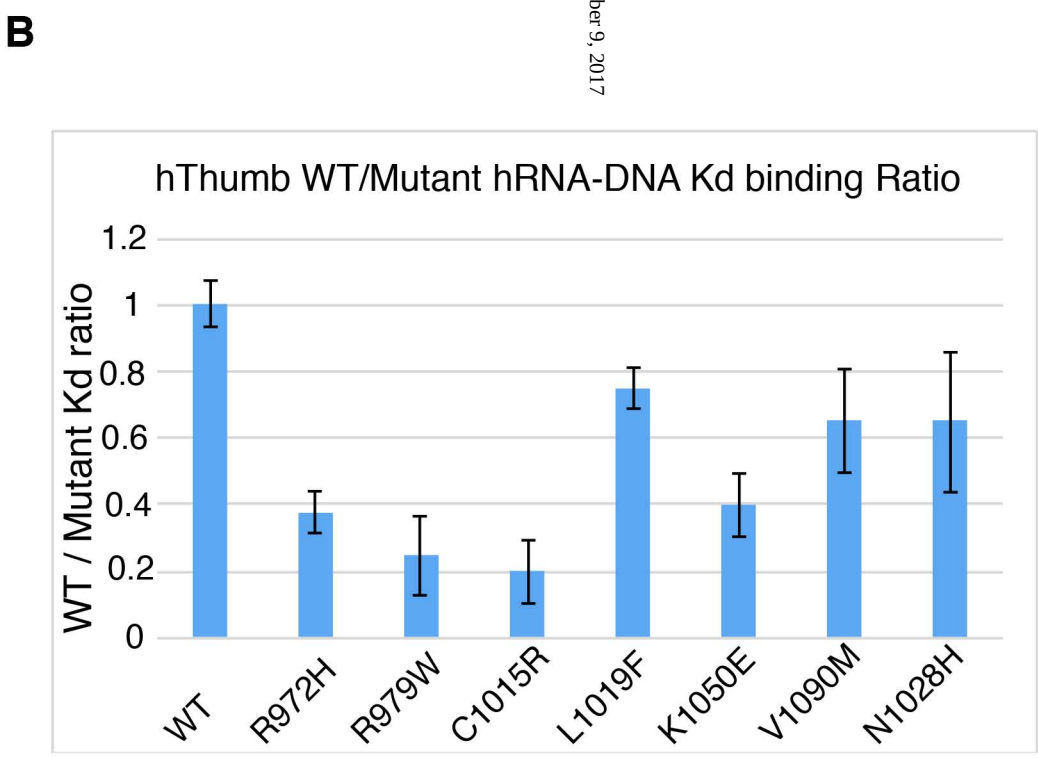

Figure 2

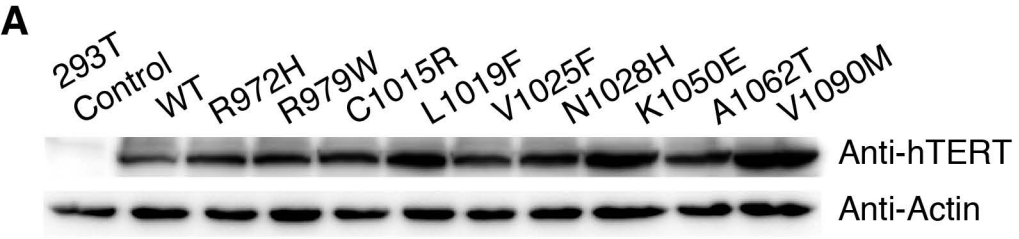

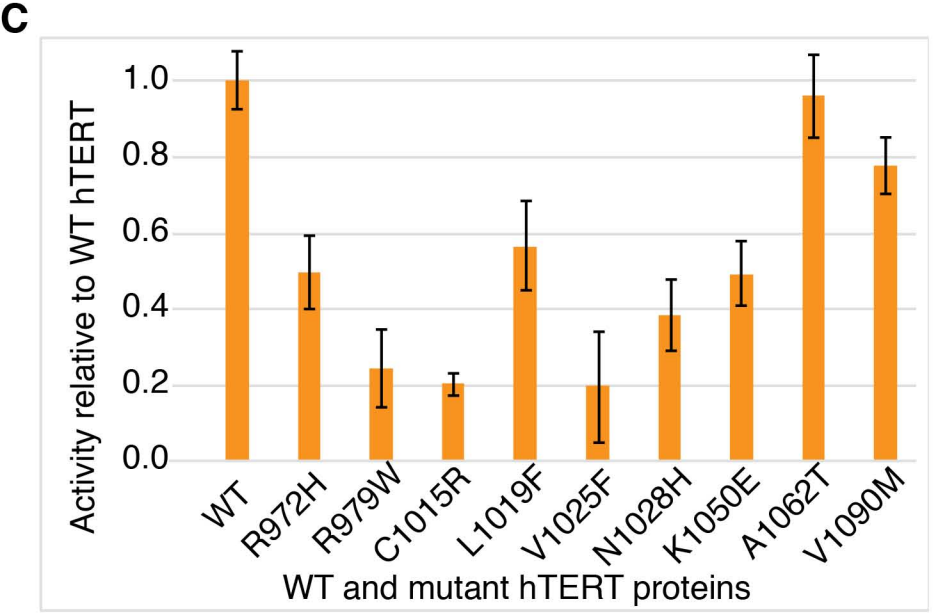

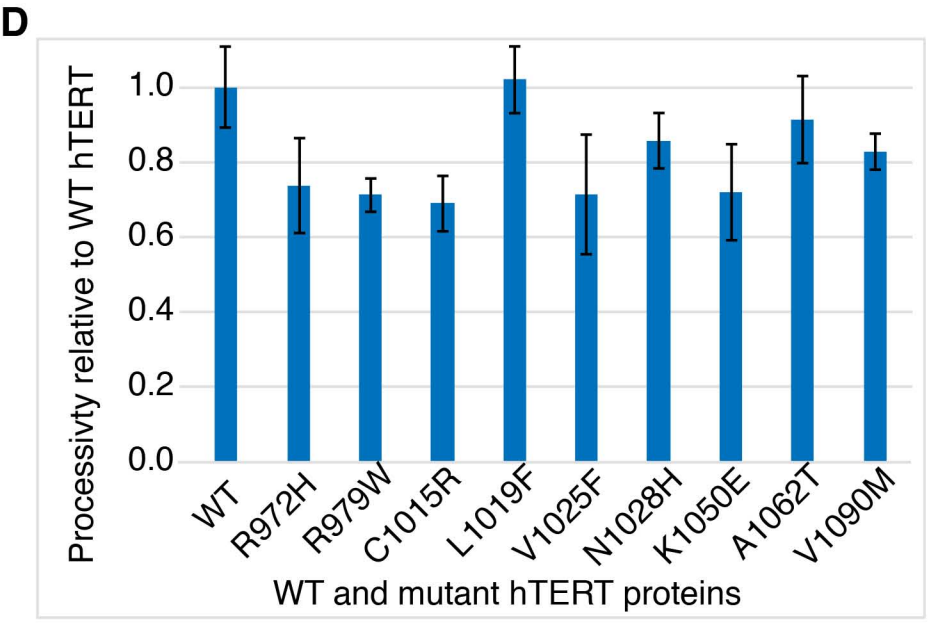

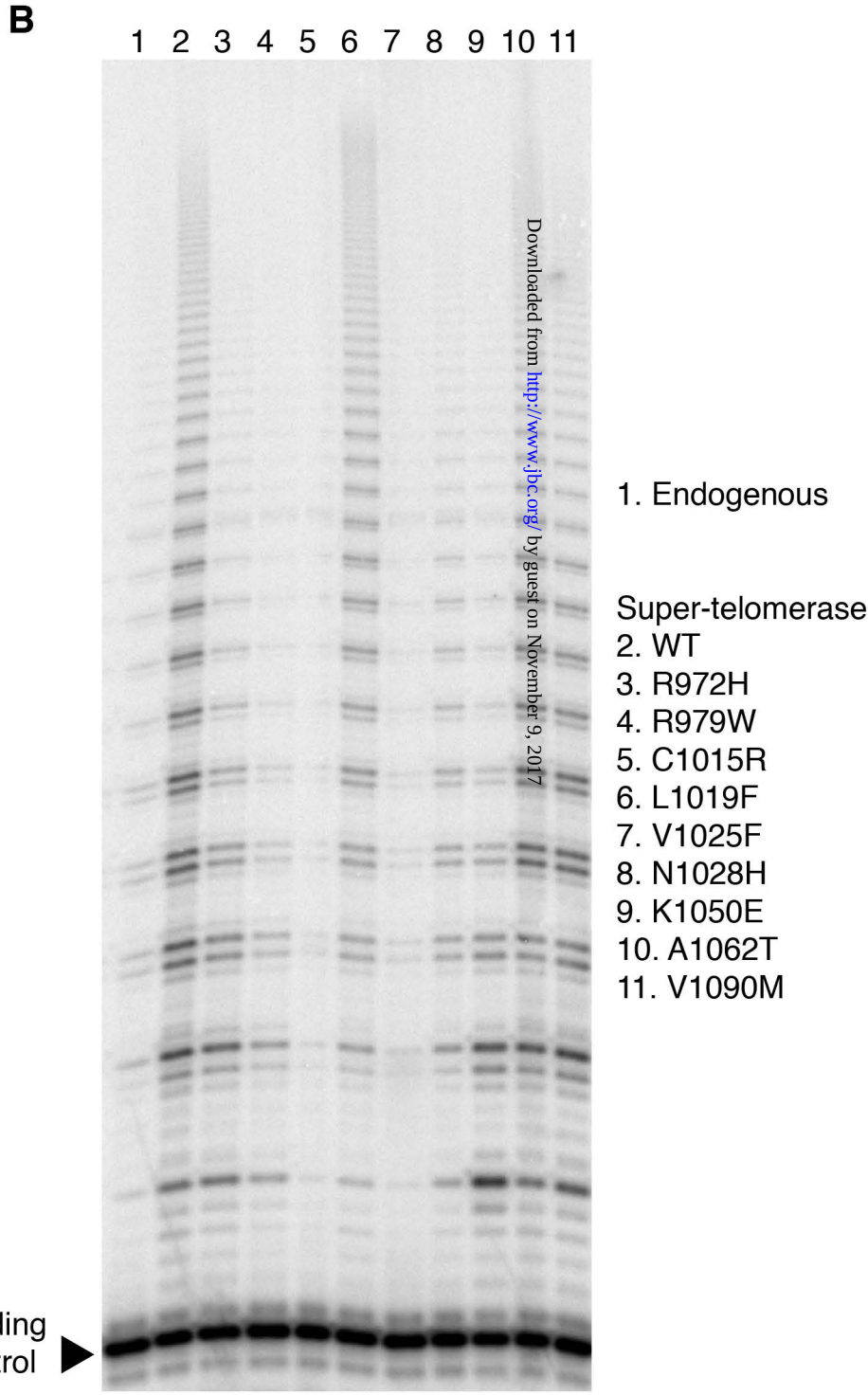

Figure 3

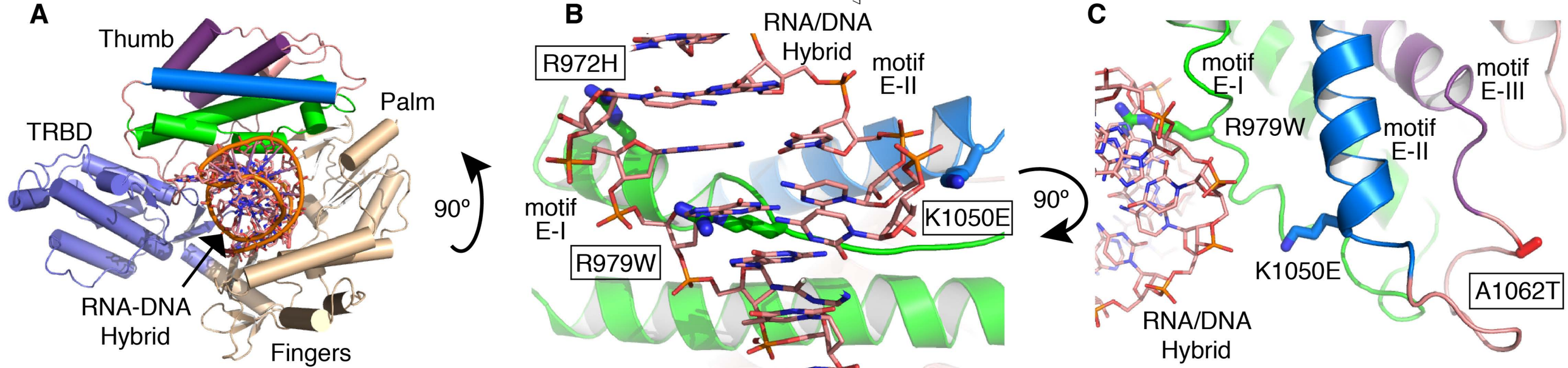
A
Thumb
Palm
TRBD
RNA-DNA
Hybrid
Fingers
90°
B
RNA/DNA
Hybrid
R972H
motif
E-II
motif
E-I
R979W
K1050E
90°
C
motif
E-I
motif
E-III
R979W
motif
E-II
K1050E
A1062T
RNA/DNA
Hybrid

Figure 4

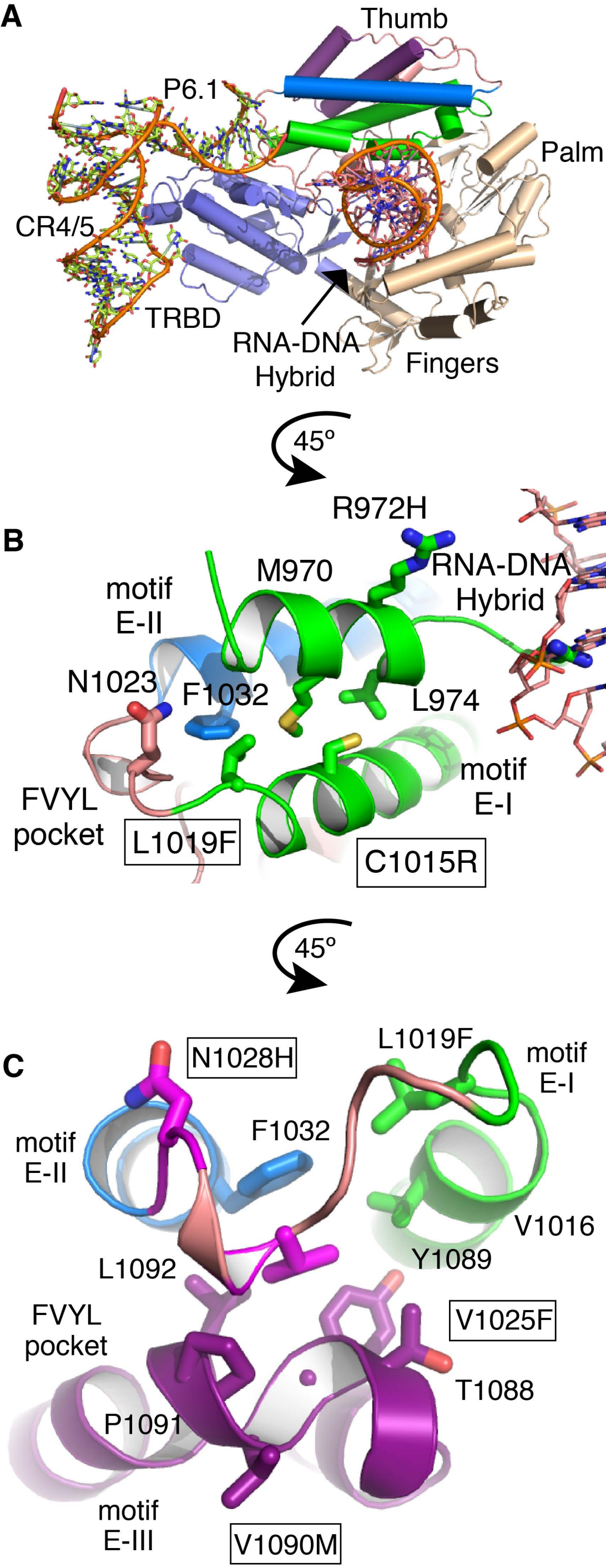
A
Thumb
P6.1
Palm
CR4/5
TRBD
RNA-DNA
Hybrid
Fingers
45°
B
R972H
M970
RNA-DNA
Hybrid
motif
E-II
N1023
F1032
L974
motif
E-I
FVYL
pocket
L1019F
C1015R
45°
C
N1028H
L1019F
motif
E-I
motif
E-II
F1032
V1016
L1092
Y1089
FVYL
pocket
V1025F
T1088
P1091
motif
E-III
V1090M

Figure 5

Structural Analysis Reveals the Deleterious Effects of Telomerase Mutations in Telomerase-Associated Bone Marrow Failure Syndromes

Hunter Hoffman, Cory Rice and Emmanuel Skordalakes

J. Biol. Chem. published online February 1, 2017
